Wacks DH, Malkeson SP, Chakraborty N.

Statistical behaviour of fuel mass fraction variance transport in turbulent flame-droplet interaction: A Direct Numerical Simulation analysis.

Numerical Heat Transfer, Part A: Applications **(2016)**

DOI: http://dx.doi.org/10.1080/10407782.2016.1230398

Statistical behaviour of fuel mass fraction variance transport in turbulent flame-droplet interaction: A Direct Numerical Simulation analysis

Daniel H. Wacks [(a)], Sean P. Malkeson[(b)], Nilanjan Chakraborty [(a)*]

[(a)]School of Mechanical and Systems Engineering, University of Newcastle, Newcastle-Upon-Tyne, NE1 7RU, United Kingdom

[(b)]MMI Engineering Ltd., The Brew House, Wilderspool Park, Greenall's Avenue, Warrington, WA4 6HL, United Kingdom

Corresponding author: nilanjan.chakraborty@ncl.ac.uk

Phone No: +44(0)191 208 3570

Fax: +44(0)191 208 8600

* Corresponding author

ABSTRACT

Three-dimensional Direct Numerical Simulations (DNS) data of statistically planar turbulent spray flames propagating into mono-disperse droplets for different values of droplet diameter a_d and droplet equivalence ratio ϕ_d has been used to analyse the statistical behaviour of the fuel mass fraction variance $\widetilde{Y_F''^2}$ and its transport in the context of Reynolds Averaged Navier-Stokes (RANS) simulations. The algebraic closure, which was previously derived for high Damköhler number turbulent stratified mixture combustion, has been shown not to capture statistical behaviour of $\widetilde{Y_F''^2}$ for turbulent spray flames, because the underlying assumptions behind the original modelling are invalid for the cases considered in this analysis. The modelling of the unclosed terms of the variance $\widetilde{Y_F''^2}$ transport equation (i.e. the turbulent transport term T_1, the reaction rate contribution T_3, the evaporation contribution T_4 and the dissipation rate term $-D_2$) has been analysed in the context of Reynolds Averaged Navier Stokes (RANS) simulations. The models previously proposed in the context of turbulent gaseous stratified flames have been considered here to assess their suitability for turbulent spray flames. Model expressions have been identified for T_1, T_4 and $-D_2$ which have been shown to perform satisfactorily in all cases considered in the current study. However, the model previously proposed for T_3 in the context of turbulent gaseous stratified flames has been found to be inadequate for turbulent spray flames and further consideration of the modelling of this unclosed term is therefore necessary.

Keywords: Turbulent droplet combustion; Fuel mass fraction variance; Reynolds Averaged Navier-Stokes simulation; Direct Numerical Simulation; Mixture fraction

NOMENCLATURE

Arabic

a_d	Droplet diameter
A	Coefficient which determines fuel mass fraction distribution on Burke-Schumann diagram
B_d	Spalding mass transfer number
c	Reaction progress variable
C_P	Specific heat at constant pressure
C_u	Correction for drag coefficient
C_v	Specific heat at constant volume
$C_{LR}, C_Y, C_\xi, C_{T_4}$	Model parameters
D	Mass diffusivity
D_0	Diffusivity in unburned gas
D_1	Molecular diffusion term in the variance transport equation
D_2	Dissipation term in the variance transport equation
Da	Damköhler number
$\tilde{k}$	Turbulent kinetic energy
L_{11}	Integral length scale for turbulent velocity fluctuation
L_V	Latent heat of droplet evaporation
m	Model parameter
Nu_c	Corrected Nusselt number for droplets
p	Pressure
p_F^S	Partial pressure at the droplet surface
$P(Y_F)$	Pdf of fuel mass fraction Y_F
$P(\xi\|Y_F)$	Pdf of mixture fraction ξ conditional on fuel mass fraction Y_F
$P(Y_F, \xi)$	Joint pdf between fuel mass fraction Y_F and mixture fraction ξ
$\widetilde{P}(Y_F, \xi)$	Favre joint pdf between fuel mass fraction Y_F and mixture fraction ξ
Pr	Prandtl number
$\bar{q}$	Reynolds averaged value of a general quantity
$\tilde{q}$	Favre averaged value of a general quantity
q''	Favre fluctuation of a general quantity
Re_d	Droplet Reynolds number
s	Ratio of oxidiser to fuel by mass under stoichiometric condition
S	Segregation factor
S_{mod}	Modified segregation factor

Sc	Schmidt number
Sh_c	Corrected Sherwood number
$S_{b(\phi_g)}$	Unstrained laminar burning velocity at equivalence ratio ϕ_g
t	Time
t_{chem}	Chemical time scale
t_e	Initial turbulent eddy turnover time
T	Non-dimensional temperature
$\hat{T}$	Dimensional Temperature
$T_{ad(\phi_g)}$	Adiabatic flame temperature
T_d	Dimensional droplet temperature
T_0	Unburned gas temperature
T_1	Turbulent transport term in the variance transport equation
T_2	Generation/Destruction term in the variance transport equation due to scalar flux
T_3	Reaction rate contribution to the variance transport equation
u_i	i^{th} component of non-dimensional fluid velocity
u'	Root mean square fluctuation velocity
$\vec{u}_d$	Droplet velocity vector
W_F, W_O	Molecular weight of fuel and oxidiser
$\vec{x}_d$	Droplet position vector
x_i	i^{th} Cartesian co-ordinate
Y_F	Fuel mass fraction
$Y_{F\infty}$	Fuel mass fraction in pure fuel stream
Y_{Fst}	Fuel mass fraction under stoichiometric condition
Y_{max} and Y_{min}	Maximum and minimum values of fuel mass fraction according to the Burke-Schumann relation
Y_O	Oxidiser mass fraction
$Y_{O\infty}$	Oxidiser mass fraction in pure air stream

Greek

α	Heat release parameter
α_T	Thermal diffusivity
α_W	Parameter in the presumed joint pdf $\widetilde{P}(Y_F, \xi)$
$\alpha_1, \alpha_2, \alpha_4$	Model parameters
$\beta_1, \beta_2, \beta_4, \beta_\epsilon$	Model parameters

γ	Ratio of specific heats of constant pressure to constant volume in gaseous phase
γ_4	Model parameter
δ_{th}	Thermal laminar premixed flame thickness for the stoichiometric mixture
$\tilde{\epsilon}$	Dissipation rate of turbulent kinetic energy
$\tilde{\epsilon}_Y$	Dissipation rate of fuel mass fraction variance
$\tilde{\epsilon}_\xi$	Dissipation rate of mixture fraction variance
η	Kolmogorov length scale
λ	Thermal conductivity of the gaseous phase
λ_W	Parameter in the presumed joint pdf $\widetilde{P}(Y_F, \xi)$
μ	Dynamic viscosity
μ_t	Eddy viscosity
ξ	Mixture fraction
ξ^{max} and ξ^{min}	Maximum and minimum values of mixture fraction within the domain of definition
ξ_{st}	Mixture fraction under stoichiometric condition
ψ, ψ_1	General primitive variable
ρ	Gas density
ρ_d	Droplet density
ρ_0	Unburned gas density
σ	Turbulent Schmidt number
τ	Heat release parameter
τ_d^p, τ_d^u and τ_d^T	Relaxation/decay timescales for droplet velocity, diameter and temperature
ϕ_d	Droplet equivalence ratio
ϕ_g	Equivalence ratio in gaseous phase
$\dot{\omega}_F$	Reaction rate of fuel
$\dot{\omega}_A$ and $\dot{\omega}_B$ ($\dot{\omega}_C$ and $\dot{\omega}_D$)	Fuel reaction rates when the fuel mass fraction values are given by Y_{F11} and Y_{F12} (Y_{F21} and Y_{F22}) respectively at a mixture fraction ξ_{41} (ξ_{42}).
Ω_Y	The term given by $[\overline{\dot{\omega}_F Y_F} - \overline{\dot{\omega}_F}\widetilde{Y}_F]$
Subscript	
d	Droplet (i.e. in liquid phase)
g	Gaseous phase
l	Liquid phase
ref	Reference value
Superscript	

g	Gaseous phase
s	Saturated state

Acronyms

DNS	Direct Numerical Simulation
RANS	Reynolds Averaged Navier Stokes

1. INTRODUCTION

The advancement in high performance computing has made Computational Fluid Dynamics (CFD) simulations a viable alternative to expensive experimentation. However, most industrial flows are turbulent in nature, and the modelling of turbulent flow remains a challenging task, but this complexity is augmented in turbulent droplet combustion simulations due to complex interaction of heat and mass transfer associated with evaporation, fluid dynamics, combustion and heat release [1-3]. Thus, the fidelity of CFD simulations of turbulent reacting flows remains sensitive to the accuracy of combustion modelling, which principally focuses on the prediction of mean chemical reaction and heat release rates. The closure of the mean reaction rate in the context of Reynolds Averaged Navier Stokes (RANS) simulations in turbulent combustion often requires knowledge of the variance of the fuel mass fraction Y_F fluctuations $\widetilde{Y_F''^2} = \overline{\rho Y_F''^2}/\bar{\rho}$ [1-5], where $\bar{q}$, $\tilde{q} = \overline{\rho q}/\bar{\rho}$ and $q'' = q - \tilde{q}$ are Reynolds average, Favre mean and Favre fluctuation of a general quantity q and ρ is the gas density. Algebraic and transport equation based closures of $\widetilde{Y_F''^2}$ have previously been considered in the context of purely gaseous phase combustion where variations in equivalence ratio exist [4-8]. Whilst previous studies on droplet combustion analysed the modelling of the mixture fraction variance $\widetilde{\xi''^2}$ [9,10], the statistical behaviour of $\widetilde{Y_F''^2}$ and its transport are yet to be examined in detail in the context of the combustion of droplet-laden mixtures. Furthermore, the validity of existing closures of $\widetilde{Y_F''^2}$ and the unclosed terms of its transport equation, which were originally proposed for purely gaseous phase combustion, is yet to be assessed for turbulent spray flames. These gaps in the existing literature have been addressed here by analysing the statistical behaviours of $\widetilde{Y_F''^2}$ and the terms of its transport equation using a three-dimensional compressible Direct Numerical Simulations (DNS) database [11] of statistically planar turbulent flames propagating into droplet-laden mixtures where the fuel is supplied in the form of mono-disperse droplets ahead of the flame. The current study considers selected cases from a large database [11] so that the effects of droplet diameter a_d and droplet equivalence ratio ϕ_d (i.e. fuel in liquid droplets to air ratio by mass, normalised by fuel to air ratio by mass under stoichiometric condition) on the statistical behaviours of $\widetilde{Y_F''^2}$ and its transport can be analysed in detail. The main objectives of this study are:

(a) To analyse the statistical behaviours of $\widetilde{Y_F''^2}$ and the various unclosed terms of its transport equation for turbulent spray flames in the context of RANS.

(b) To assess the validity of the existing models for the unclosed terms of $\widetilde{Y_F''^2}$ transport equation for turbulent droplet combustion.

The rest of the paper will be organised as follows. The mathematical background and numerical implementation pertinent to this analysis are presented in the next section. This will be followed by the presentation of results and their subsequent discussion. Finally, the main findings will be summarised and conclusions will be drawn.

2. MATHEMATICAL BACKGROUND & NUMERICAL IMPLEMENTATION

A modified single-step irreversible chemical mechanism [12] was used to perform the present analysis: $\text{Fuel} + s \cdot \text{Oxidiser} \rightarrow (1+s) \cdot \text{Products}$, where s is the oxidiser-fuel ratio by mass under stoichiometric condition. The activation energy and heat of combustion are taken to be functions of the gaseous equivalence ratio, ϕ_g, so that a realistic ϕ_g dependence of unstrained laminar burning velocity can be obtained [12]. All species are taken to have unity Lewis number and are assumed to be perfect gases. Standard values have been taken for the ratio of specific heats ($\gamma = 1.4$) and Prandtl number ($\text{Pr} = 0.7$) for the gaseous phase. The individual droplets are tracked in Lagrangian sense and the quantities transported for each droplet are the position, $\vec{x}_d$, velocity, $\vec{u}_d$, diameter, a_d and temperature, T_d. The transport equations of $\vec{x}_d$, $\vec{u}_d$, a_d and T_d are given as [9,11,13-16]:

$$\frac{d\vec{x}_d}{dt} = \vec{u}_d \;\; ; \; \frac{d\vec{u}_d}{dt} = \frac{\vec{u}(\vec{x}_d,t)-\vec{u}_d}{\tau_d^p} \; ; \; \frac{da_d^2}{dt} = -\frac{a_d^2}{\tau_d^u} \text{ and } \frac{dT_d}{dt} = -\frac{\hat{T}(\vec{x}_d,t)-T_d-B_d L_v/C_P^g}{\tau_d^T} \tag{1i}$$

where L_v is the latent heat of vaporization, and τ_d^p, τ_d^u and τ_d^T are relaxation/decay timescales for droplet velocity, diameter and temperature respectively, which are defined as:

$$\tau_d^p = \frac{\rho_d a_d^2}{18 C_u \mu} \; ; \; \tau_d^u = \frac{\rho_d a_d^2}{4\mu}\frac{Sc}{Sh_c}\frac{1}{\ln(1+B_d)} \text{ and } \tau_d^T = \frac{\rho_d a_d^2}{6\mu}\frac{Pr}{Nu_c}\frac{B_d}{\ln(1+B_d)}\frac{C_p^L}{C_p^g} \tag{1ii}$$

where ρ_d is the droplet density, C_p^L is the specific heat for the liquid phase, C_p^g is the specific heat at constant pressure for the gaseous phase, C_u is the corrected drag coefficient and is given by:

$$C_u = 1 + \frac{1}{6}\text{Re}_d^{2/3} \tag{1iii}$$

Furthermore, Re_d is the droplet Reynolds number, Sc is the Schmidt number, B_d is the Spalding mass transfer number, Sh_c is the corrected Sherwood number and Nu_c is the corrected Nusselt number, which are defined as [9,11,13-16]:

$$\text{Re}_d = \frac{\rho|\vec{u}(\vec{x}_d,t)-\vec{u}_d|a_d}{\mu} \; ; \; B_d = \frac{Y_F^s - Y_F(\vec{x}_d,t)}{1-Y_F^s} \text{ and } Sh_c = Nu_c = 2 + \frac{0.555\text{Re}_d Sc}{\left(1.232+\text{Re}_d Sc^{4/3}\right)^{1/2}} \tag{1iv}$$

where Y_F^s is the value of Y_F at the surface of the droplet. Equation 1iv implicitly invoke the unity Lewis number assumption. The Clausius–Clapeyron relation for the partial pressure of the fuel vapour at the droplet surface, p_F^s, is used to evaluate the Spalding number B_d, which leads to:

$$p_F^s = p_{ref}\exp\left(\frac{L_v}{R_0}\left[\frac{1}{T_{ref}^s}-\frac{1}{T_d^s}\right]\right); \; Y_F^s = \left(1+\frac{W_O}{W_F}\left[\frac{p(\vec{x}_d,t)}{p_F^s}-1\right]\right)^{-1} \tag{1v}$$

where T_{ref}^s is the boiling point of the fuel at pressure p_{ref}, R_0 is the universal gas constant, T_d^s is assumed to be T_d, and W_O and W_F are the molecular weights of oxidiser and fuel respectively.

The droplet and gaseous phases are coupled in the gaseous transport equations [12,14,16-19]:

$$\rho(D\psi/Dt) = \nabla\cdot\left(\Gamma_\psi \nabla\psi_1\right) + \dot{\omega}_\psi + \dot{S}_g + \dot{S}_\psi \tag{1vi}$$

where $\psi = \{1, u_j, e, Y_F, Y_O\}$ for the conservation of mass, momentum, energy and mass fractions respectively, $\psi_1 = \{1, u_j, \hat{T}, Y_F, Y_O\}$ for $\psi = \{1, u_j, e, Y_F, Y_O\}$, and $\Gamma_\psi = \mu/\sigma_\psi$ and λ for $\psi = \{u_j, Y_F, Y_O\}$ and $\psi = e$ respectively, with u_j , μ , λ and σ_ψ being the velocity component in the j^{th} direction, dynamic viscosity, thermal conductivity and an appropriate Schmidt number for ψ respectively. The term $\dot{\omega}_\psi$ arises due to chemical reaction rate and $\dot{S}_g$ is an appropriate gaseous phase source term. The droplet source term arising from evaporation, $\dot{S}_\psi = -1/V \sum_d d(m_d \psi_d)/dt$, is interpolated from the droplet's sub-grid position to the 8 surrounding nodes, where V is the cell volume, $m_d = \rho_d (1/6)\pi a_d^3$ is the droplet mass and the summation is carried out over all droplets in the vicinity of each node [9,11,13-16].

Droplet evaporation leads to mixture inhomogeneities, which are characterized by the mixture fraction: $\xi = (Y_F - Y_O/s + Y_{O\infty}/s)/(Y_{F\infty} + Y_{O\infty}/s)$, where $Y_{F\infty} = 1.0$ $(Y_{O\infty} = 0.233)$ is the fuel (oxidiser) mass fraction in the pure fuel (air) stream. The fuel used here is n-heptane, C_7H_{16}, for which $s = 3.52$ and the stoichiometric fuel mass/mixture fraction is: $Y_{Fst} = \xi_{st} = 0.0621$. Using ξ a reaction progress variable c can be defined in the following manner [11,13-15]: $c = [(1-\xi)Y_{O\infty} - Y_O]/[(1-\xi)Y_{O\infty} - \max(0, [\xi_{st} - \xi]/\xi_{st})Y_{O\infty}]$ so that c increases monotonically from 0 in unburned reactants to 1.0 in fully burned products. Using Eq. 1vi one obtains the following transport equation for $\widetilde{Y_F''^2}$ [8]:

$$\partial\left(\bar{\rho}\widetilde{Y_F''^2}\right)/\partial t + \partial\left(\bar{\rho}\tilde{u}_j\widetilde{Y_F''^2}\right)/\partial x_j = \partial\left(\bar{\rho}\tilde{D}(\partial\widetilde{Y_F''^2}/\partial x_j)\right)\Big/\partial x_j \underbrace{-\partial\left(\overline{\rho u_j'' Y_F''^2}\right)/\partial x_j}_{T_1 - turbulent\ transport}$$
$$\underbrace{-2\overline{\rho u_j'' Y_F''}(\partial\widetilde{Y_F}/\partial x_j)}_{T_2 - mean\ scalar\ gradient\ term} + \underbrace{2\left(\overline{\dot{\omega}_F Y_F} - \overline{\dot{\omega}_F}\widetilde{Y_F}\right)}_{T_3 - reaction\ term} + \underbrace{\overline{(2Y_F - Y_F^2)\Gamma} - \left(2\widetilde{Y_F} - \widetilde{Y_F}^2\right)\bar{\Gamma}}_{T_4 - evaporation\ term} - \tag{2}$$

where $\widetilde{\epsilon_Y} = [(\overline{\rho D\left(\partial Y_F''/\partial x_j\right)\left(\partial Y_F''/\partial x_j\right)})]/\bar{\rho}$ is the Favre-averaged scalar dissipation rate (SDR) of Y_F and Γ is the source term in the mass conservation equation due to evaporation. The term $(-D_2)$ is responsible for dissipation of $\widetilde{Y_F''^2}$. The terms of T_1, T_3, T_4 and $(-D_2)$ are unclosed terms in the context of second-moment closure and their modelling will be discussed in Section 3.

The present study uses a three-dimensional compressible DNS code SENGA [9,11,13-15]. High-order finite-difference (i.e. 10^{th} central difference scheme for the internal grid points and the order of differentiation gradually reduces to a 2^{nd} order one-sided scheme at the non-periodic boundaries) and explicit 3^{rd} order low storage Runge-Kutta schemes are used for spatial differentiation and time advancement respectively. A rectangular domain of size $63.35D_0/S_{b(\phi_g=1)} \times 42.17D_0/S_{b(\phi_g=1)} \times 42.17D_0/S_{b(\phi_g=1)}$ has been considered, where D_0 and $S_{b(\phi_g=1)}$ are the unburned gas diffusivity and the unstrained laminar burning velocity of the stoichiometric mixture respectively. For the present thermo-chemistry $D_0/S_{b(\phi_g=1)} \approx 0.625\delta_{th}$ where $\delta_{th} = \left(T_{ad(\phi_g=1)} - T_0\right)/\max\left(|\nabla\hat{T}|\right)_L$ is the

unstrained thermal laminar flame thickness of the stoichiometric laminar premixed flame, where subscript L refers to the values in the unstrained stoichiometric laminar premixed flame. The simulation domain is discretised using a Cartesian grid of size $384 \times 256 \times 256$, ensuring that both the flame thickness, δ_{th}, and the Kolmogorov length-scale, η, are resolved. The boundaries in the mean direction of flame propagation (i.e. x-direction) are considered to be partially non-reflecting, whereas the other boundaries are taken to be periodic. The boundary conditions are specified using the well-known Navier Stokes Characteristic Boundary Conditions (NSCBC) technique [17]. The droplets are distributed uniformly in space throughout the y- and z-directions and in the region $0.0 \leq xS_{b(\phi_g=1)}/D_0 \leq 16.53$ ahead of the flame. The reacting flow field is initialised based on the steady laminar solution generated using COSILAB [18] for desired values of a_d and ϕ_d, as done previously by Neophytou and Mastorakos [19] for one-dimensional laminar spray flame simulations. Initial turbulent velocity fluctuations, generated using a standard pseudo-spectral method [20] following Batchelor-Townsend spectrum [21], have been superimposed on top of the steady laminar spray flame solution. For the present analysis the unburned gas temperature is taken as $T_0 = 300$K, which leads to $\tau = (T_{ad(\phi_g=1)} - T_0)/T_0 = 6.54$ where $T_{ad(\phi_g=1)}$ is the adiabatic flame temperature of the stoichiometric mixture. The fuel is supplied purely in the form of mono-disperse droplets with $a_d/\delta_{th} = 0.06, 0.08, 0.10$ for different values of $\phi_d = 1.0, 1.25, 1.5, 1.7$ at a distance $16.53\, D_0/S_{b(\phi_g=1)}$ from the point in the laminar flame at which $\widehat{T} = 400$K. The initial droplet number density ρ_N varies between $1.16 \leq (\rho_N)^{1/3}\delta_{th} \leq 2.27$ in the region $0.0 \leq xS_{b(\phi_g=1)}/D_0 \leq 16.53$ and the liquid volume fraction remains well below 0.01. Droplets are supplied at the left-hand-side boundary to maintain a constant ϕ_d ahead of the flame. Due to the high volatility of n-heptane, evaporation commences on entry and the droplet diameter decreases by at least 40%, 30% and 25% by the time it reaches the most reactive region of the flame for the initial $a_d/\delta_{th} = 0.06, 0.08, 0.10$ cases respectively, such that the volume of even the largest droplets remains smaller than half that of the cell volume, which validates the sub-grid point source treatment of droplets adopted for flame-droplet interactions analysed here. The droplet diameter to grid size used in the current analysis remains comparable to several previous DNS analyses [9,10,13-16].

The cases considered here have initial values of normalised root-mean-square (rms) turbulent velocities $u'/S_{b(\phi_g=1)} = 7.5$ and non-dimensional longitudinal integral length-scale $L_{11}/\delta_{th} = 2.5$. The ratio of droplet diameter to the Kolmogorov scale is $a_d/\eta \approx 0.3, 0.4, 0.5$ for $a_d/\delta_{th} \approx 0.06, 0.08, 0.1$ respectively for initial $u'/S_{b(\phi_g=1)} = 7.5$. The mean normalised inter-droplet distance s_d/η ranges between 0.0220 and 0.0432. All simulations have been carried out until $t_{final} = \max(3t_{turb}, 4t_{chem})$, where $t_{turb} = L_{11}/u'$ and $t_{chem} = D_0/S^2_{b(\phi_g=1)}$ are the initial eddy turnover time and chemical time, respectively. The simulation time remains either greater than or comparable to several previous analyses [13-15,22-25]. The volume-integrated reaction rate, flame surface area and burning rate per unit area were not changing rapidly when the statistics have been extracted [11].

The Reynolds/Favre averaged values of a quantity Q (i.e. $\overline{Q}$ and $\widetilde{Q}$) are evaluated by ensemble-averaging Q over the y-z plane at a given x-location.

3. RESULTS & DISCUSSION

Figures 1ai-iii present the instantaneous distributions of normalised fuel mass fraction Y_F/Y_{Fst}, mixture fraction ξ and non-dimensional temperature $T = (\widehat{T} - T_0)/(T_{ad(\phi_g=1)} - T_0)$ (where $\widehat{T}$ is the instantaneous dimensional temperature) fields in the central $x - z$ plane for $a_d/\delta_{th} = 0.08$ and $\phi_d = 1.0$ at $t = 4t_{chem}$, where the black dots indicate the droplets which reside immediately adjacent to the plane. The droplets shrink due to evaporation as they approach the flame, but may not completely evaporate until after passing through the flame. The evaporating droplets absorb latent heat from the background gas (this occurs on both sides of the flame, but is more noticeable on the burned gas side). In many cases, the evaporation of droplets is not complete on their arrival at the flame front, the reaction takes place predominantly under fuel-lean conditions and, therefore, the resultant burned gas temperature are lower than the adiabatic flame temperature of the stoichiometric mixture (i.e. $T < 1.0$) [11]. The predominant fuel-lean combustion in these cases suggests a slow combustion process and low values of Damköhler number Da (i.e. $Da = L_{11}S_{b(\phi_g)}^2/u'D_0 < 1$) [11].

Mura *et al.* [6] approximated the Favre joint PDF between Y_F and ξ (i.e. $\widetilde{P}(Y_F, \xi) = \rho P(Y_F, \xi)/\overline{\rho}$) for turbulent stratified gaseous mixture combustion as:

$$\widetilde{P}(Y_F, \xi) = \lambda_w \widetilde{P}(\xi|Y_{max})\delta\big(Y_F - Y_{max}(\xi)\big) + (1 - \lambda_w)\widetilde{P}(\xi|Y_{min})\delta\big(Y_F - Y_{min}(\xi)\big) + O(1/Da) \quad (3)$$

where $\widetilde{P}(\xi|Y_F)$ is the Favre PDF of ξ conditional on Y_F and the quantities $Y_{max}(\xi) = \xi$ and $Y_{min}(\xi) = A(\xi)(\xi - \xi_{st})$ are maximum and minimum values of Y_F according to the Burke-Schumann relations [26] where $A(\xi) = H(\xi - \xi_{st})/(1 - \xi_{st})$ with $H(\xi - \xi_{st})$ being a Heaviside function. For $Da \gg 1$ the last term on the right hand side of eq. 3 disappears and λ_w is unlikely to depend on ξ, which yields $\widetilde{P}(\xi|Y_{max}) = \widetilde{P}(\xi|Y_{min})$ [6]. The contours of Favre joint PDFs of Y_F and ξ at $\tilde{c} = 0.1, 0.3, 0.5$ for $a_d/\delta_{th} = 0.06$, $\phi_d = 1.0$ are shown in Figs. 1bi-iii and the same qualitative behaviour has been observed for other cases. Figures 1bi-iii indicate that $\widetilde{P}(Y_F, \xi)$ in these cases cannot be accurately approximated by discrete delta functions as suggested by eq. 3 due to low Da effects.

Figures 2ai-iii show the variations of $\widetilde{Y}_F$, $\widetilde{Y}_{max} = \tilde{\xi}$ and $\widetilde{Y}_{min} = H(\widetilde{\xi - \xi_{st}})/(1 - \xi_{st})$ with $\tilde{c}$ across the flame-brush for all cases considered in this paper. In all cases $\widetilde{Y}_F$ remains smaller than Y_{Fst} across the flame-brush indicating predominant fuel-lean combustion. Furthermore, $\widetilde{Y}_F$ remains small at $\tilde{c} = 0$ as the fuel is supplied purely in the form of droplets and gaseous fuel becomes available only with the evaporation of droplets as the flame is approached. In all cases $\widetilde{Y}_F$ attains a peak value somewhere in the middle of the flame-brush before decreasing towards the burned gas side due to the consumption of the gaseous fuel. The peak value of $\widetilde{Y}_F$ reduces and shifts towards the burned

gas side of the flame-brush for increasing values of a_d as the evaporation rate is slower for the larger droplets. For $\phi_d = 1.0$ cases the value of $\widetilde{Y}_F$ vanishes at $\tilde{c} = 1$ as the fuel droplets have predominantly been evaporated within the flame-brush and the fuel is subsequently consumed. However, for $\phi_d = 1.7$ cases the droplets continue to evaporate towards the burned gas side of the flame-brush and evaporation increases towards the reaction zone of the flame (i.e. $0.7 < \tilde{c} < 0.9$). Therefore, $\widetilde{Y}_F$ begins to rise again towards $\tilde{c} = 1$ for these cases. The value of $\widetilde{Y}_{max} = \tilde{\xi}$ has been found to rise with $\tilde{c}$ across the flame-brush as the fuel droplets evaporate, but it remains smaller than ξ_{st} for all $\phi_d = 1.0$ cases. However, towards the burned gas side of the flame-brush $\widetilde{Y}_{max} > \xi_{st}$ for $\phi_d = 1.7$ cases, although the extent of this reduces as a_d increases. The value of $\widetilde{Y}_{min} \approx 0.0$ for all $\phi_d = 1.0$ cases due to predominant fuel-lean combustion, but $\widetilde{Y}_{min} > 0.0$ has been observed towards the burned gas side of the flame-brush for $\phi_d = 1.70$ cases. The variations of $\widetilde{Y}_F$, $\widetilde{Y}_{max}$ and $\widetilde{Y}_{min}$ play key roles in the algebraic closure proposed by Mura *et al.* [6] for $\widetilde{Y_F''^2}$ under the assumption of $Da \gg 1$:

$$\widetilde{Y_F''^2} = \left(\widetilde{Y}_{max} - \widetilde{Y}_F\right)\left(\widetilde{Y}_F - \widetilde{Y}_{min}\right) + \underbrace{\left[\left(\widetilde{Y}_F - \widetilde{Y}_{min}\right)/\left(\widetilde{Y}_{max} - \widetilde{Y}_{min}\right) + \left\{\left(\widetilde{Y}_{max} - \widetilde{Y}_F\right)/\left(\widetilde{Y}_{max} - \widetilde{Y}_{min}\right)\right\}\widetilde{A}^2\right]\widetilde{\xi''^2}}_{Q_{s1}} \quad (4)$$

Equation 4 is obtained using $\widetilde{Y}_F = \int\int Y_F \widetilde{P}(Y_F, \xi) dY_F d\xi$ and $\widetilde{Y_F''^2} = \int\int \left(Y_F - \widetilde{Y}_F\right)^2 \widetilde{P}(Y_F, \xi) dY_F d\xi$ which also imply $\lambda_W = \left(\widetilde{Y}_F - \widetilde{Y}_{min}\right)/\left(\widetilde{Y}_{max} - \widetilde{Y}_{min}\right)$. The second term on the right hand side of eq. 4 originates due to mixture inhomogeneity. Figures 2bi-iii present the variations of $\widetilde{Y_F''^2}$ and $\widetilde{\xi''^2}$ with $\tilde{c}$, which show that $\widetilde{\xi''^2}$ remains larger than $\widetilde{Y_F''^2}$ in all cases across the flame-brush (most noticeably for high values of a_d), except for the case with small a_d and ϕ_d where $\widetilde{Y_F''^2} > \widetilde{\xi''^2}$ towards the centre of the flame-brush. There is a clear effect on the general behaviour of $\widetilde{Y_F''^2}$ and $\widetilde{\xi''^2}$ due to a_d, as evaporation of the fuel droplets continues to occur towards the burned gas side of the flame-brush for the large droplet cases. Figures 2bi-iii show that eq. 4 captures neither the quantitative nor qualitative behaviour of $\widetilde{Y_F''^2}$. As mentioned above Figs. 1bi-iii show that $\widetilde{P}(Y_F, \xi)$ cannot be adequately represented by eq. 3 here and therefore eq. 4 does not satisfactorily predict $\widetilde{Y_F''^2}$.

Mura *et al.* [6] defined a segregation factor S as: $S = \left\{\widetilde{Y_F''^2} - \left[\left(\widetilde{Y}_F - \widetilde{Y}_{min}\right)/\left(\widetilde{Y}_{max} - \widetilde{Y}_{min}\right) + \left\{\left(\widetilde{Y}_{max} - \widetilde{Y}_F\right)/\left(\widetilde{Y}_{max} - \widetilde{Y}_{min}\right)\right\}\widetilde{A}^2\right]\widetilde{\xi''^2}\right\}/\left[\left(\widetilde{Y}_{max} - \widetilde{Y}_F\right)\left(\widetilde{Y}_F - \widetilde{Y}_{min}\right)\right]$. One obtains negative values of $Q_{s2} = \widetilde{Y_F''^2} - Q_{s1}$ and S, if $Q_{s1} = \left\{\left[\left(\widetilde{Y}_F - \widetilde{Y}_{min}\right)/\left(\widetilde{Y}_{max} - \widetilde{Y}_{min}\right) + \left\{\left(\widetilde{Y}_{max} - \widetilde{Y}_F\right)/\left(\widetilde{Y}_{max} - \widetilde{Y}_{min}\right)\right\}\widetilde{A}^2\right]\widetilde{\xi''^2}\right\}$ becomes greater than $\widetilde{Y_F''^2}$. Figures 2bi-iii show the variations of Q_{s1} and Q_{s2} with $\tilde{c}$ across the flame-brush which indicate that Q_{s2} assumes negative values towards the unburned gas side of the flame-brush in all cases and the extent of this negative value increases with increasing a_d. Note that ξ is strictly not a passive scalar in spray combustion, because evaporation leads to an extra source/sink term in its transport equation. Thus, the Burke-Schumann relations [26]

(where ξ is strictly a passive scalar), based on which the expressions of $\widetilde{Y}_{max}$, $\widetilde{Y}_{min}$ and S have been obtained, may not be valid for spray combustion. From the foregoing it can be inferred that it may be necessary to consider a modelled transport equation of $\widetilde{Y_F''^2}$ in the absence of a satisfactory algebraic closure.

The variations of the terms T_1, T_2, T_3, T_4 and $(-D_2)$ (see eq. 2) with $\tilde{c}$ across the flame-brush are shown in Fig. 3, which indicates that non-zero values are observed at $\tilde{c} = 0$ because of mixture inhomogeneity for all terms except T_3. Figure 3 shows that the magnitudes of T_1 and T_2 remain small in comparison to the other terms. The reaction rate contribution term T_3 has been found to be a significant contributor to $\widetilde{Y_F''^2}$ transport, but its magnitude remains smaller than the evaporation and molecular dissipation terms (i.e. T_4 and $-D_2$). The reaction rate term T_3 assumes predominantly positive values for the major part of the flame-brush, although some negative values have been observed towards $\tilde{c} = 0$ and $\tilde{c} = 1$. The magnitude of T_3 has been found to increase with increasing ϕ_d due to stronger chemical reaction arising from greater availability of fuel. The evaporation term T_4 has been found to be a leading-order source term, whereas the dissipation rate term $(-D_2)$ remains the leading-order sink across the flame-brush for all cases. The magnitudes of T_4 and $(-D_2)$ remain large at the leading edge (i.e. $\tilde{c} \approx 0$), but they diminish with increasing $\tilde{c}$ before increasing again due to stronger evaporation within the flame until a "peak" value is obtained within the flame-brush before falling again towards the trailing edge (i.e. $\tilde{c} \approx 1$) of the flame as the droplets are evaporated and the fuel is consumed within the flame-brush.

Figure 3 shows that the magnitudes of T_4 and $(-D_2)$ are significantly affected by both ϕ_d and a_d. The magnitudes of T_4 and $(-D_2)$ increase with increasing ϕ_d due to a higher amount of evaporated fuel vapour in the gaseous phase which in turn increases $|\nabla Y_F|$. The evaporation rate increases with decreasing a_d and, therefore, the magnitudes of T_4 and $(-D_2)$ reach their "peak" values closer to the leading edge of the flame-brush for the smaller droplets which show faster evaporation rate. These observations and the underlying physics must be accounted for when modelling these unclosed terms.

The mean scalar gradient term T_2 has been found to exhibit both positive and negative values indicating a combination of gradient (i.e. $\overline{\rho u_1'' Y_F''}\left(\partial \widetilde{Y_F}/\partial x_1\right) < 0$) and counter-gradient (i.e. $\overline{\rho u_1'' Y_F''}\left(\partial \widetilde{Y_F}/\partial x_1\right) > 0$) transport. As the term T_2 is closed in the context of second-moment closure, the modelling of T_1, T_3, T_4 and $(-D_2)$ will be addressed next in this paper. However, the accuracy of the evaluation of the term T_2 depends on the modelling of turbulent scalar flux $\overline{\rho u_j'' Y_F''}$ which is beyond the scope of the present study.

The modelling of the turbulent transport term T_1 in statistically planar flames translates to the closure of $\overline{\rho u_1'' Y_F''^2}$. The quantity $\overline{\rho u_1'' Y_F''^2}$ is often modelled using the gradient hypothesis as [4,5]: $\overline{\rho u_i'' Y_F''^2} = -(\mu_t/\sigma)\,\partial \widetilde{Y_F''^2}/\partial x_i$ where $\mu_t = 0.09\bar{\rho}\tilde{k}^2/\tilde{\epsilon}$ is the eddy viscosity, σ is a turbulent Schmidt number, $\tilde{k}$ is the turbulent kinetic energy and

$\tilde{\epsilon}$ is its dissipation rate. However, it is known that $\overline{\rho u_1'' Y_F''^2}$ can exhibit counter-gradient behaviour, thus it will be desirable to have a model which can predict both gradient and counter-gradient transport [8]. Previously, an expression for $\overline{\rho u_1'' Y_F''^2}$ was proposed by using eq. 3 and the identity $\overline{\rho u_1'' Y_F''^2} = \bar{\rho}\int\int\int(u_1 - \tilde{u}_1)(Y_F - \tilde{Y}_F)^2 \tilde{P}(Y_F, \xi) du_1 dY_F d\xi$ in the following manner [8], which is capable of predicting both gradient and counter-gradient transport:

$$\overline{\rho u_1'' Y_F''^2} = \left[2\left(\tilde{Y}_{Fmax} - \tilde{Y}_F\right) - \left(\tilde{Y}_{Fmax} - \tilde{Y}_{Fmin}\right)\right]\left[\overline{\rho u_1'' Y_F''} - \lambda_W \overline{\rho u_1'' \xi''} - (1 - \lambda_W)\widetilde{A}\overline{\rho u_1'' \xi''}\right] + \lambda_W \overline{\rho u_1'' \xi''^2} + (1 - \lambda_W)\widetilde{A}\overline{\rho u_1'' \xi''^2} \quad (5)$$

The predictions of $\overline{\rho u_1'' Y_F''^2} = -(\mu_t/\sigma)\,\partial\widetilde{Y_F''^2}/\partial x_1$ and eq. 5 are shown in Fig. 4 along with the variations of $\overline{\rho u_1'' Y_F''^2}$ obtained from DNS data. Figure 4 shows that $-(\mu_t/\sigma)\,\partial\widetilde{Y_F''^2}/\partial x_1$ satisfactorily captures the quantitative behaviour of $\overline{\rho u_1'' Y_F''^2}$ in all cases for $\sigma = 1.0$. Although eq. 5 captures the general qualitative behaviour, it over-predicts the magnitude of $\overline{\rho u_1'' Y_F''^2}$ for the major part of the flame-brush. As eq. 5 is derived based on eq. 3 which is strictly valid for $Da \gg 1$ combustion, it is perhaps not surprising that eq. 5 does not provide accurate predictions for $Da < 1$ cases considered here. To address this shortcoming eq. 5 was modified in the following manner [8]:

$$\overline{\rho u_1'' Y_F''^2} = \left[2\left(\tilde{Y}_{Fmax} - \tilde{Y}_F\right)S_{Mod}^m - \left(\tilde{Y}_{Fmax} - \tilde{Y}_{Fmin}\right)\right](2S_{Mod}/S_{Mod} + 1) \times \left[\overline{\rho u_1'' Y_F''} - \lambda_W \overline{\rho u_1'' \xi''} - (1 - \lambda_W)\widetilde{A}\overline{\rho u_1'' \xi''}\right] + \lambda_W \overline{\rho u_1'' \xi''^2} + (1 - \lambda_W)\widetilde{A}\overline{\rho u_1'' \xi''^2} \quad (6)$$

where $m = 0.1\,\tilde{\xi}(1 - \xi_{st})/[\xi_{st}(1 - \tilde{\xi})]$ is a model parameter, and $S_{Mod} = \max(0, S)$ is the modified segregation factor in order to eliminate unphysical negative values of segregation factor (see Fig. 2). Equation 6 becomes identical to eq. 5 for $Da \gg 1$ combustion where $S_{mod} = 1.0$. Figure 4 shows that eq. 6 satisfactorily captures the behaviour of $\overline{\rho u_1'' Y_F''^2}$ throughout the flame-brush.

The modelling of T_3 is dependent upon the accurate modelling of the quantity $\Omega_Y = [\overline{\dot{\omega}_F Y_F} - \overline{\dot{\omega}_F}\tilde{Y}_F]$ [4]. Robin *et al.* [5] proposed a closure for $\Omega_Y = [\overline{\dot{\omega}_F Y_F} - \overline{\dot{\omega}_F}\tilde{Y}_F]$ using the following presumed distribution of $\tilde{P}(Y_F, \xi)$:

$$\tilde{P}(Y_F, \xi) = \alpha_4 \tilde{P}_1(Y_F)\delta(\xi - \xi_{41}) + (1 - \alpha_4)\tilde{P}_2(Y_F)\delta(\xi - \xi_{42}) \quad (7)$$

where $\tilde{P}_1(Y_F) = \beta_4\delta(Y_F - Y_{F11}) + (1 - \beta_4)\delta(Y_F - Y_{F12})$ and $\tilde{P}_2(Y_F) = \gamma_4\delta(Y_F - Y_{F21}) + (1 - \gamma_4)\delta(Y_F - Y_{F22})$ and α_4, β_4 and γ_4 are: $\alpha_4 = (\xi^{max} - \xi)/(\xi^{max} - \xi^{min})$ $\beta_4 = (Y_{F1}^{max} - \tilde{Y}_{F1})/(Y_{F1}^{max} - Y_{F1}^{min})$ and $\gamma_4 = (Y_{F2}^{max} - \tilde{Y}_{F2})/(Y_{F2}^{max} - Y_{F2}^{min})$. According to Robin *et al.* [5] the quantities $\xi_{41}, \xi_{42}, Y_{F1}$ and Y_{F2} are given by: $\xi_{41} = \tilde{\xi} - \left[((1 - \alpha_4)/\alpha_4)\widetilde{\xi''^2}\right]^{1/2}$; $\xi_{42} = \tilde{\xi} + \left[(\alpha_4/(1 - \alpha_4))\widetilde{\xi''^2}\right]^{1/2}$; $Y_{F1} = \tilde{Y}_F - \left[((1 - \alpha_4)/\alpha_4)\widetilde{Y_F''^2}\right]^{1/2}$ and $Y_{F2} = \tilde{Y}_F + \left[(\alpha_4/(1 - \alpha_4))\widetilde{Y_F''^2}\right]^{1/2}$. The quantities $Y_{F11}, Y_{F12}, Y_{F21}$ and Y_{F22} in the expressions for $\tilde{P}_1(Y_F)$ and $\tilde{P}_2(Y_F)$ are given by [7]: $Y_{F11} = \tilde{Y}_{F1} - \left[((1 - \beta_4)/\beta_4)\widetilde{Y_{F1}''^2}\right]^{1/2}$; $Y_{F12} = \tilde{Y}_{F1} + \left[(\beta_4/(1 - \beta_4))\widetilde{Y_{F1}''^2}\right]^{1/2}$; $Y_{F21} = \tilde{Y}_{F2} - \left[((1 - \gamma_4)/\gamma_4)\widetilde{Y_{F2}''^2}\right]^{1/2}$ and $Y_{F22} = \tilde{Y}_{F2} + \left[(\gamma_4/(1 - \gamma_4))\widetilde{Y_{F2}''^2}\right]^{1/2}$. The quantities ξ^{max} and ξ^{min} are the maximum

and minimum values of ξ within the domain of definition and Y_{F1}^{max} and Y_{F1}^{min} (Y_{F2}^{max} and Y_{F2}^{min}) are the maximum and minimum values of fuel mass fraction respectively at ξ_{41} (ξ_{42}) [5]. The variances $\widetilde{Y_{F1}''^2}$ and $\widetilde{Y_{F2}''^2}$ are evaluated using the relations: $\widetilde{Y_F''^2} + \widetilde{Y}_F^2 = \alpha_4\left(\widetilde{Y_{F1}''^2} + \widetilde{Y}_{F1}^2\right) + (1-\alpha_4)(\widetilde{Y_{F2}''^2} + \widetilde{Y}_{F2}^2)$ and $\widetilde{Y_{F1}''^2}/\widetilde{Y_{F2}''^2} = (Y_{F1}^{max} - \widetilde{Y}_{F1})(\widetilde{Y}_{F1} - Y_{F1}^{min})/[(Y_{F2}^{max} - \widetilde{Y}_{F2})(\widetilde{Y}_{F2} - Y_{F2}^{min})]$ [5]. According to eq. 7, Ω_Y can be expressed as [5]:

$$\Omega_Y = \alpha_4\beta_4\dot{\omega}_A Y_{F11} + \alpha_4(1-\beta_4)\dot{\omega}_B Y_{F12} + (1-\alpha_4)\gamma_4\dot{\omega}_C Y_{F21} + (1-\alpha_4)(1-\gamma_4)\dot{\omega}_D Y_{F22}$$
$$-[\alpha_4\beta_4\dot{\omega}_A + \alpha_4(1-\beta_4)\dot{\omega}_B + (1-\alpha_4)\gamma_4\dot{\omega}_C + (1-\alpha_4)(1-\gamma_4)\dot{\omega}_D]\widetilde{Y}_F \quad (8)$$

where $\dot{\omega}_A$ and $\dot{\omega}_B$ ($\dot{\omega}_C$ and $\dot{\omega}_D$) are the fuel reaction rates when the fuel mass fraction values are given by Y_{F11} and Y_{F12} (Y_{F21} and Y_{F22}) respectively at a mixture fraction ξ_{41} (ξ_{42}) [5]. The predictions of $\Omega_Y = \overline{\dot{\omega}_F Y_F} - \overline{\dot{\omega}_F}\widetilde{Y}_F$ according to eq. 8 are shown in Fig. 5, which indicates that this model does not adequately capture both qualitative and quantitative variations of Ω_Y obtained from DNS data. However, a reasonable level of agreement is observed towards the burned gas side of the flame-brush for $\phi_d = 1.0$. It should be stressed, however, that the model by Robin *et al.* [5] was proposed in the context of turbulent gaseous stratified flames with $Da \gg 1$ where $\widetilde{P}(Y_F, \xi)$ can be approximated by eq. 7. It has already been shown in Fig. 1 that $\widetilde{P}(Y_F, \xi)$ cannot sufficiently be approximated by eq. 7. Furthermore, eq. 8 implicitly assumes Burke-Schumann relations [26] and considers ξ to be a passive scalar, which are not strictly valid in spray flames. Thus, shortcomings of this model for turbulent spray flames with predominantly $Da < 1$ combustion are not unexpected.

Figure 3 shows that the evaporation term T_4 is a leading-order contributor to $\widetilde{Y_F''^2}$ transport for all cases considered here. As a first attempt, T_4 has been modelled in the following manner: $T_4 = \bar{\rho}C_{T_4}(\tilde{\epsilon}/\tilde{k})\widetilde{\xi''^2}$ where C_{T4} is a model parameter. Figure 6 shows that $\bar{\rho}C_{T_4}(\tilde{\epsilon}/\tilde{k})\widetilde{\xi''^2}$ predicts T_4 satisfactorily when C_{T4} is taken to be $C_{T4} = 9.0$.

Equation 2 indicates that the modelling of $(-D_2)$ is dependent upon the accurate evaluation of $\tilde{\epsilon}_Y$. A linear relaxation model: $\tilde{\epsilon}_Y = C_{LR}(\tilde{\epsilon}/\tilde{k})\widetilde{Y_F''^2}$ (where C_{LR} is a model parameter) is often used which is denoted here as the LR-SDY model. Mura *et al.* [6] proposed an alternative model for $\tilde{\epsilon}_Y$ for turbulent stratified flames as:

$$\tilde{\epsilon}_Y = S_{Mod}\left(-\overline{\rho D}\frac{\partial\widetilde{Y}_F}{\partial x_k}\frac{\partial\widetilde{Y}_F}{\partial x_k} - \frac{\bar{\dot{\omega}}_F}{2}\left(\widetilde{Y}_{max} - \widetilde{Y}_F + \widetilde{Y}_{min}\right) + \left[\overline{\dot{\omega}_F Y_F} - \bar{\dot{\omega}}_F\widetilde{Y}_F\right]\right)\frac{1}{\bar{\rho}}$$
$$+S_{Mod}\left(\frac{\widetilde{Y}_F - \widetilde{Y}_{min}}{\widetilde{Y}_{max} - \widetilde{Y}_{min}} + \frac{\widetilde{Y}_{max} - \widetilde{Y}_F}{\widetilde{Y}_{max} - \widetilde{Y}_{min}}\widetilde{A^2}\right) \times \tilde{\epsilon}_\xi + (1 - S_{Mod})C_Y\frac{\tilde{\epsilon}}{\tilde{k}}\widetilde{Y_F''^2} \quad (9)$$

where C_Y is a model parameter. The predictions of eq. 9 with $\bar{\dot{\omega}}_F$ and $\Omega_Y = [\overline{\dot{\omega}_F Y_F} - \overline{\dot{\omega}_F}\widetilde{Y}_F]$ extracted from DNS and according to eq. 8 are shown in Fig. 7 where they are referred to as SDRY-M1 and SDRY-M2 respectively. Figure 7 shows whilst the LR-SDY model captures the general qualitative behaviour of $\tilde{\epsilon}_Y$, the model parameter C_{LR} needs to be tuned in order to obtain satisfactory quantitative agreement, whereas the SDRY-M1 and SDRY-M2 models follow the general behaviour of $\tilde{\epsilon}_Y$ across the flame-brush reasonably well when C_Y is taken to be $C_Y = 6.0$. Note that the predictions of the SDRY-M1 and SDRY-M2 models cannot be separated from each other for

$a_d/\delta_{th} = 0.08$ and 0.1 cases (see Figs. 7b and c), which suggests that the contributions of $\bar{\dot{\omega}}_F$ and $\Omega_Y = [\overline{\dot{\omega}_F Y_F} - \overline{\dot{\omega}_F}\widetilde{Y}_F]$ do not play major roles in the prediction of eq. 9 in these cases, where the evaporation rates (and Damköhler number) are smaller than in the $a_d/\delta_{th} = 0.06$ cases.

4. CONCLUSIONS

The statistical behaviours of $\widetilde{Y_F''^2}$ and the unclosed terms of its transport equation have been analysed using three-dimensional DNS of statistically planar turbulent flames for which the fuel is supplied in the form of mono-disperse droplets for different a_d and ϕ_d. An algebraic closure based on presumed distribution of $\widetilde{P}(Y_F, \xi)$ which was originally intended for high Damköhler number gaseous phase combustion does not adequately predict $\widetilde{Y_F''^2}$ obtained from DNS data. The behaviours of the unclosed terms of $\widetilde{Y_F''^2}$ transport equation have been analysed in the context of RANS simulations. It has been found that the reaction rate, evaporation and molecular dissipation contributions (i.e. T_3, T_4 and $-D_2$) play significant roles in $\widetilde{Y_F''^2}$ transport. The suitability of the models previously proposed in the context of turbulent gaseous stratified flames have been assessed for the modelling of $\widetilde{Y_F''^2}$ transport in turbulent spray flames. Based on *a-priori* DNS analysis suitable model expressions have been identified for T_1, T_4 and $(-D_2)$, which have been shown to perform satisfactorily for all cases considered here. However, a model previously proposed for T_3 for turbulent stratified flames has been found not to perform satisfactorily. Thus, further consideration of the modelling of $\widetilde{Y_F''^2}$ transport equation for spray flames is necessary. Moreover, the effects of detailed chemistry are not considered in the current study. Therefore, future research in these directions will be necessary for a comprehensive assessment of the model performances. Furthermore, the implementation of the proposed models in actual RANS simulations will be necessary for *a-posteriori* assessment.

ACKNOWLEDGEMENTS

The authors are grateful to EPSRC UK and N8/ARCHER for financial and computational support respectively.

REFERENCES

1. A.K. Tolpadi, S. K. Agarwal, H.C. Mongia, An advanced spray model for application to the prediction of gas turbine combustor flow fields, *Numer. Heat Trans. A*, vol. **38**, pp. 325-340, 2000.

2. F. M. Ashayek, G.B. Jacobs, Temperature-dependent reaction in droplet-laden homogeneous turbulence, *Numer. Heat Trans. A*, vol. **39**, pp. 101-121, 2001.

3. K. Li, L.X. Zhou, Studies of the effect of spray inlet conditions on the flow and flame structures of ethanol-spray combustion by Large-Eddy Simulation, *Numer. Heat Trans. A*, vol. **62**, pp. 44-59, 2012.

4. G. Ribert, M. Champion, O. Gicquel, N. Darabiha, D. Veynante, Modeling nonadiabatic turbulent premixed reactive flows including tabulated chemistry, *Combust. Flame*, vol. **141**, pp. 271–280, 2005.

5. V. Robin, A. Mura, M. Champion, P. Plion, A multi-Dirac presumed PDF model for turbulent reacting flows with variable equivalence ratio, *Combust. Sci. Technol.*, vol. **178**, pp. 1843–1870, 2006.

6. A. Mura, V. Robin, M. Champion, Modeling of scalar dissipation in partially premixed turbulent flames, *Combust. Flame*, vol. **149**, pp. 217-224, 2007.

7. S. P. Malkeson, N. Chakraborty, A-priori Direct Numerical Simulation analysis of algebraic models of variances and scalar dissipation rates for Reynolds Averaged Navier Stokes Simulations for low Damköhler number turbulent partially-premixed combustion, *Combust. Sci. Technol.* vol. **182**, pp. 960–999, 2010.

8. S.P. Malkeson, N. Chakraborty, The modeling of fuel mass fraction variance transport in turbulent stratified flames: A Direct Numerical Simulation study, *Numer. Heat Trans. A.*, vol. **58**(3), pp. 187-206, 2010.

9. J. Réveillon, L. Vervisch, Spray vaporization in non-premixed turbulent combustion modelling: a single droplet model, *Combust. Flame*, vol. **121**, pp. 75-90, 2000.

10. S. Sreedhara, Kang Y. Huh, Conditional statistics of nonreacting and reacting sprays in turbulent flows by direct numerical simulation, *Proc. Combust. Inst.*, vol. **31** , pp. 2335-2342, 2007.

11.D. Wacks, N. Chakraborty, E. Mastorakos, Statistical analysis of turbulent flame-droplet interaction: A Direct Numerical Simulation Study, *Flow Turb. Combust.*, vol. **96**, pp. 573-607, 2016.

12. E. Tarrazo, A. Sanchez, A. Linan, F. Williams, A simple one-step chemistry model for partially premixed hydrocarbon combustion, *Combust. Flame*, vol. **147**, pp. 32-38, 2006.

13. A. Wandel, N. Chakraborty, E. Mastorakos, Direct Numerical Simulation of turbulent flame expansion in fine sprays , *Proc. Combust. Inst.*, vol. **32**, pp. 2283-2290, 2009.

14. A. Wandel, Extinction predictors in turbulent sprays, *Proc. Combust. Inst.*, vol. **34**, pp. 1625-1632, 2013.

15. A. Wandel, Influence of scalar dissipation on flame success in turbulent sprays with spark ignition, *Combust. Flame*, vol. **161**, pp. 2579-2600, 2014.

16. Y. Wang, C.J. Rutland, Effects of temperature and equivalence ratio on the ignition of n-heptane fuel spray in turbulent flow, *Proc. Combust. Inst.* , vol. **30**, pp. 893-900, 2005.

17. T. Poinsot, S.K. Lele, Boundary conditions for direct simulation of compressible viscous flows, *J. Comput. Phys*., vol. **101**,pp.104-129, 1992.

18. Rotexo-Softpredict-Cosilab, GmbH and Co. KG Bad Zwischenahn, Germany.

19. A. Neophytou, E. Mastorakos, Simulations of laminar flame propagation in droplet mists. *Combust. Flame*, vol. **156**, pp. 1627-1640, 2009.

20. R.S. Rogallo, Numerical experiments in homogeneous turbulence, *NASA Technical Memorandum 81315*, NASA Ames Research Center, 1981.

21. G.K. Batchelor and A.A. Townsend, Decay of Turbulence in the Final Period, *Proc. Roy. Soc. A*, vol. **194**, pp. 527-543, 1948.

22. I. Han, K.H. Huh, Roles of displacement speed on evolution of flame surface density for different turbulent intensities and Lewis numbers in turbulent premixed combustion, *Combust. Flame*., vol. **152**, pp. 194-205, 2008.

23. H. Reddy, J. Abraham, Two-Dimensional Direct Numerical Simulation Evaluation of the Flame Surface Density Model for Flames Developing from an Ignition Kernel in Lean Methane/Air Mixtures Under Engine Conditions, *Phys. Fluids*, vol. **24**,105108, 2012.

24. C. Pera, S. Chevillard, J. Reveillon, Effects of residual burnt gas heterogeneity on early flame propagation and on cyclic variability in spark-ignited engines, *Combust. Flame*, vol. **160**, pp. 1020-1032, 2013.

25. C. Dopazo, L. Cifuentes, J. Martin, C. Jimenez, Strain rates normal to approaching iso-scalar surfaces in a turbulent premixed flame, *Combust. Flame*, vol. **162**, 1729-1736, 2014.

26. T. Poinsot, D. Veynante, Theoretical and Numerical Combustion. R.T. Edwards, Philadelphia, U.S.A., 2001.

FIGURE CAPTIONS

Fig. 1: (a) Instantaneous fields of (i) normalized fuel mass fraction, Y_F/Y_{Fst}, (ii) normalised temperature T with c isolines (left to right $c = 0.1,0.3,0.5,0.7,0.9$) in white and (iii) mixture fraction ξ fields at the central $x - z$ plane at $t = 4.0t_{chem}$ for case $a_d/\delta_{th} = 0.08, \phi_d = 1.0$. Droplets are shown by black dots (not to scale). The stoichiometric mixture fraction is $\xi_{st} = 0.0621$. (b) The contours of Favre joint PDF $\widetilde{P}(Y_F, \xi)$ at (i) $\tilde{c} = 0.1$, (ii) $\tilde{c} = 0.3$ and (iii) $\tilde{c} = 0.5$ for case $a_d/\delta_{th} = 0.06, \phi_d = 1.0$. Value rises from blue to red.

Fig. 2: Variation of (a) $\widetilde{Y}_F/Y_{Fst}$, $\widetilde{Y}_{Fmax}/Y_{Fst}$ and $\widetilde{Y}_{Fmin}/Y_{Fst}$ [black, red, green], and (b) $\widetilde{Y_F''^2}/Y_{Fst}^2$, $\widetilde{\xi''^2}/Y_{Fst}^2$, Q_{S1}/Y_{Fst}^2, Q_{S2}/Y_{Fst}^2 and (model of $\widetilde{Y_F''^2}/Y_{Fst}^2$) $\times$ 0.1 based on Eq. 4 [black, red, blue, green, tan] with $\tilde{c}$ for $a_d/\delta_{th} =$ (i) 0.06, (ii) 0.08, (iii) 0.10 and $\phi_d = 1.0$ (solid line), 1.7 (dashed line with crosses).

Fig. 3: Variation of $(T_1, T_2, T_3, T_4$ and $-D_2) \times D_0/\rho_0 Y_{Fst}^2 S_{b(\phi_g=1)}^2$ [black, red, blue, green, tan] with $\tilde{c}$ for $a_d/\delta_{th} =$ (a) 0.06, (b) 0.08, (c) 0.10 and $\phi_d = 1.0$ (solid line), 1.7 (dashed line with crosses).

Fig. 4: Variation of $\overline{\rho u_1'' Y_F''^2}/\rho_o Y_{Fst}^2 S_{b(\phi_g=1)}$ and the predictions of $[-\mu_t \ \partial\widetilde{Y_F''^2}/\partial x_1]$, Eqs. 5 and 6 [black, red, blue, green] with $\tilde{c}$ for $a_d/\delta_{th} =$ (a) 0.06, (b) 0.08, (c) 0.10 and $\phi_d = 1.0$ (solid line), 1.7 (dashed line with crosses).

Fig. 5: Variation of $\Omega_Y \times D_0/\rho_0 Y_{Fst}^2 S_{b(\phi_g=1)}^2$ [black] and the prediction of Eq. 8 [red] with $\tilde{c}$ for $a_d/\delta_{th} =$ (a) 0.06, (b) 0.08, (c) 0.10 and $\phi_d = 1.0$ (solid line), 1.7 (dashed line with crosses).

Fig. 6: Variation of $T_4 \times D_0/\rho_0 Y_{Fst}^2 S_{b(\phi_g=1)}^2$ [black] and the prediction of $\bar{\rho} C_{T_4} (\tilde{\epsilon}/\tilde{k}) \widetilde{\xi''^2}$ (for $C_{T_4} = 9.0$) [red] with $\tilde{c}$ for $a_d/\delta_{th} =$ (a) 0.06, (b) 0.08, (c) 0.10 and $\phi_d = 1.0$ (solid line), 1.7 (dashed line with crosses).

Fig. 7: Variation $\tilde{\epsilon}_Y \times D_0/Y_{Fst}^2 S_{b(\phi_g=1)}^2$ [black] and the predictions of SDY-LR, SDR-M1 and SDR-M2 [red, blue, green] with $\tilde{c}$ for $a_d/\delta_{th} =$ (a) 0.06, (b) 0.08, (c) 0.10 and $\phi_d = 1.0$ (solid line for DNS, SDY-LR and SDR-M2, and solid line with diamonds for SDR-M1), 1.7 (dashed line with crosses for DNS, SDY-LR and SDR-M2, and dashed line with circles for SDR-M1).

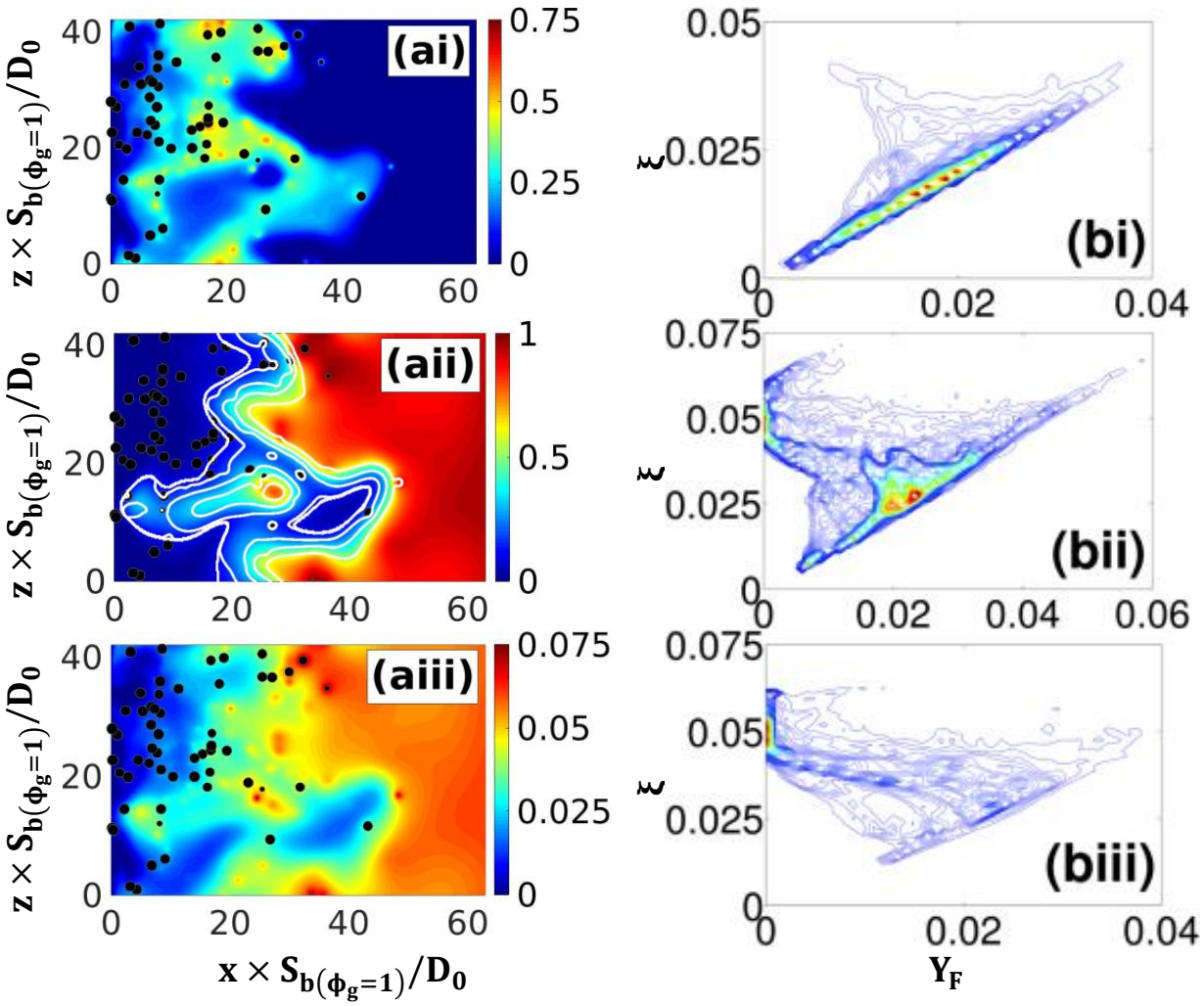

Fig. 1: (a) Instantaneous fields of (i) normalized fuel mass fraction, Y_F/Y_{Fst}, (ii) normalised temperature T with c isolines (left to right $c = 0.1, 0.3, 0.5, 0.7, 0.9$) in white and (iii) mixture fraction ξ fields at the central $x - z$ plane at $t = 4.0t_{chem}$ for case $a_d/\delta_{th} = 0.08, \phi_d = 1.0$. Droplets are shown by black dots (not to scale). The stoichiometric mixture fraction is $\xi_{st} = 0.0621$. (b) The contours of Favre joint PDF $\widetilde{P}(Y_F, \xi)$ at (i) $\tilde{c} = 0.1$, (ii) $\tilde{c} = 0.3$ and (iii) $\tilde{c} = 0.5$ for case $a_d/\delta_{th} = 0.06, \phi_d = 1.0$. Value rises from blue to red.

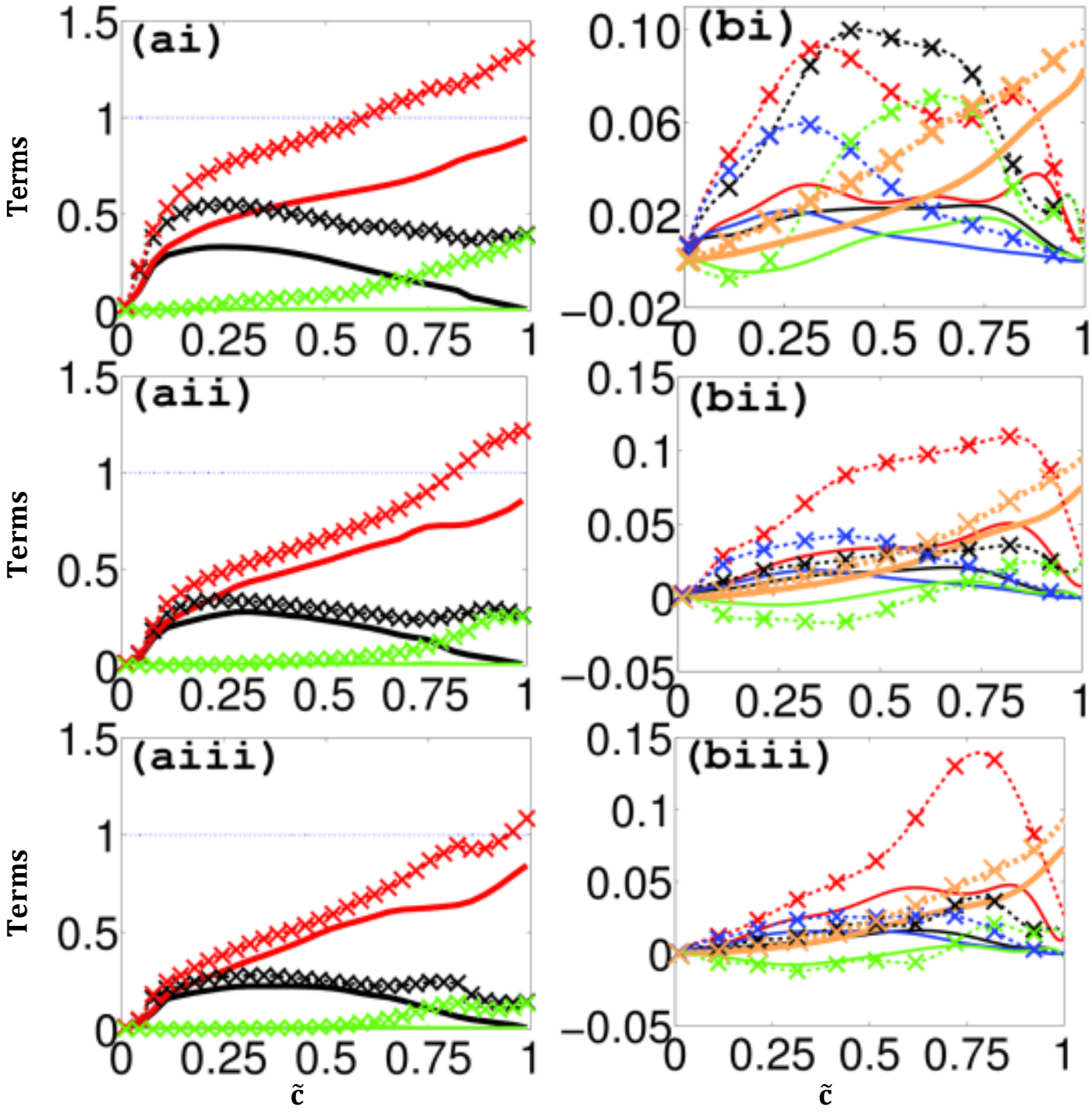

Fig. 2: Variation of (a) $\widetilde{Y}_F/Y_{Fst}$, $\widetilde{Y}_{Fmax}/Y_{Fst}$ and $\widetilde{Y}_{Fmin}/Y_{Fst}$ [black, red, green], and (b) $\widetilde{Y_F''^2}/Y_{Fst}^2$, $\widetilde{\xi''^2}/Y_{Fst}^2$, Q_{S1}/Y_{Fst}^2, Q_{S2}/Y_{Fst}^2 and (model of $\widetilde{Y_F''^2}/Y_{Fst}^2$) $\times$ 0.1 based on Eq. 4 [black, red, blue, green, tan] with $\tilde{c}$ for a_d/δ_{th} = (i) 0.06, (ii) 0.08, (iii) 0.10 and ϕ_d = 1.0 (solid line), 1.7 (dashed line with crosses).

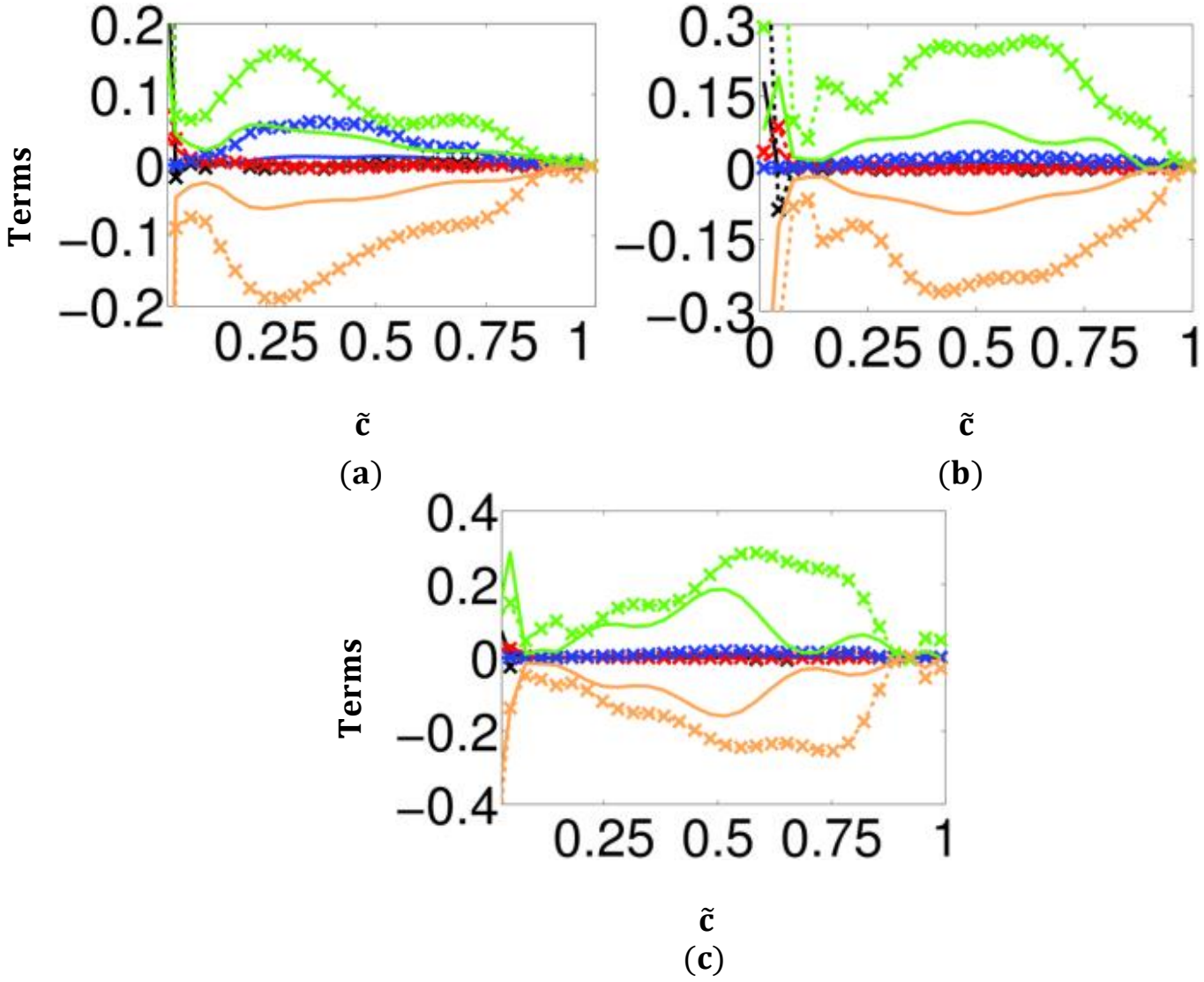

Fig. 3: Variation of $(T_1, T_2, T_3, T_4$ and $-D_2) \times D_0/\rho_0 Y_{Fst}^2 S_{b(\phi_g=1)}^2$ [black, red, blue, green, tan] with $\tilde{c}$ for $a_d/\delta_{th} = (a)\ 0.06, (b)\ 0.08, (c)\ 0.10$ and $\phi_d = 1.0$ (solid line), 1.7 (dashed line with crosses).

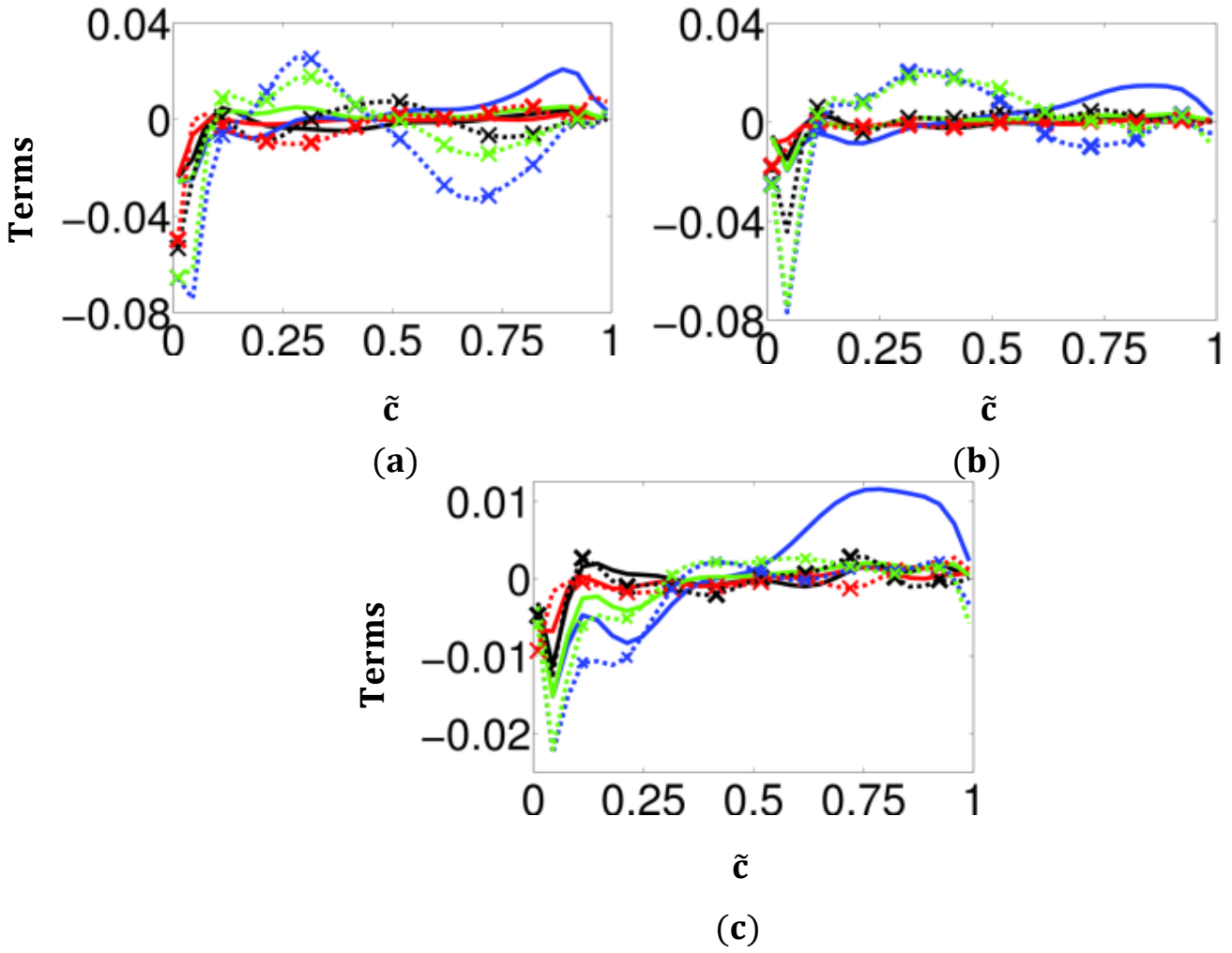

Fig. 4: Variation of $\overline{\rho u_1'' Y_F''^2}/\rho_o Y_{Fst}^2 S_{b(\phi_g=1)}$ and the predictions of $[-\mu_t\, \partial \widetilde{Y_F''^2}/\partial x_1]$, Eqs. 5 and 6 [black, red, blue, green] with $\tilde{c}$ for $a_d/\delta_{th} =$ (a) 0.06, (b) 0.08, (c) 0.10 and $\phi_d = 1.0$ (solid line), 1.7 (dashed line with crosses).

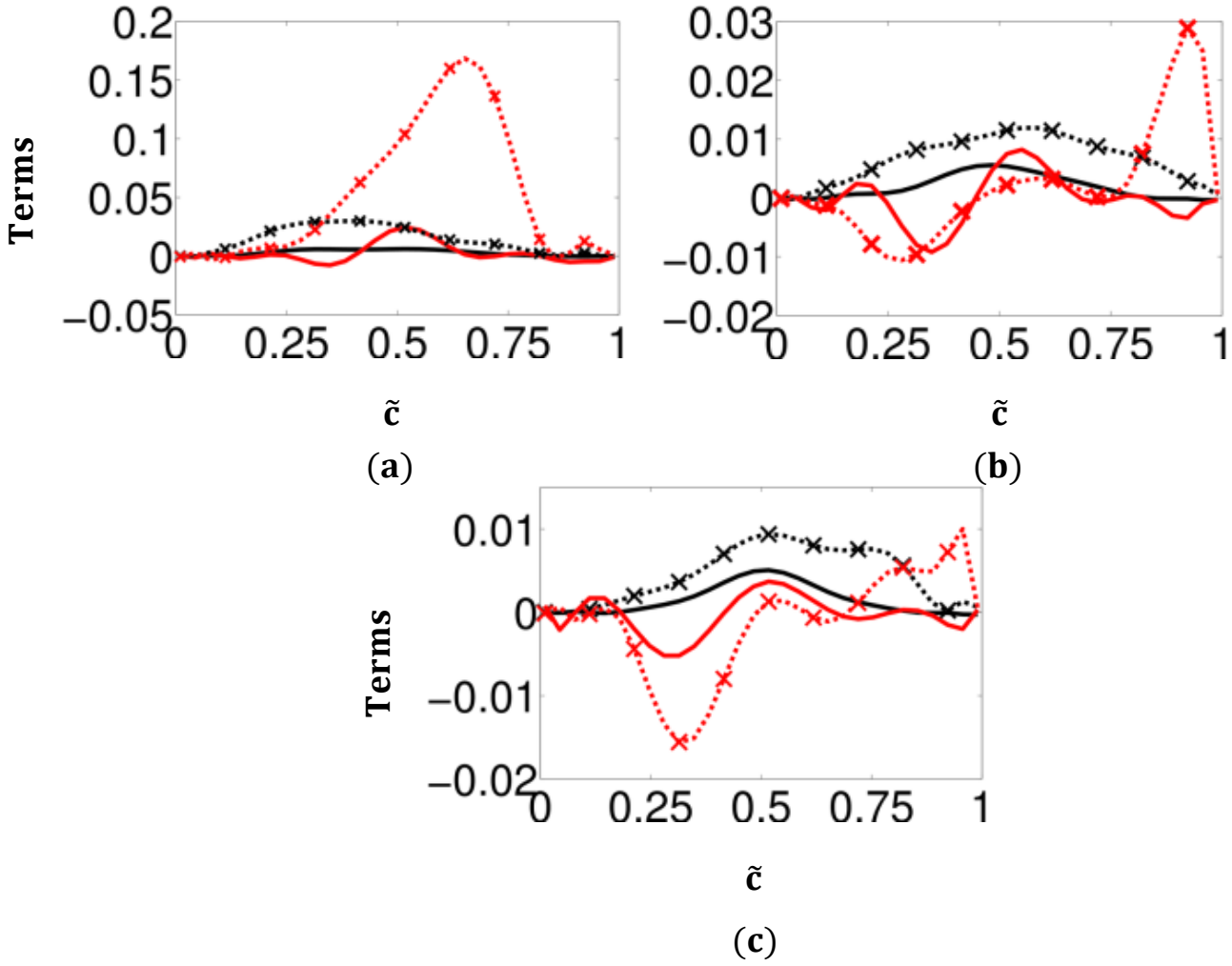

Fig. 5: Variation of $\Omega_Y \times D_0/\rho_0 Y_{Fst}^2 S_{b(\phi_g=1)}^2$ [black] and the prediction of Eq. 8 [red] with $\tilde{c}$ for $a_d/\delta_{th} =$ (a) 0.06, (b) 0.08, (c) 0.10 and $\phi_d = 1.0$ (solid line), 1.7 (dashed line with crosses).

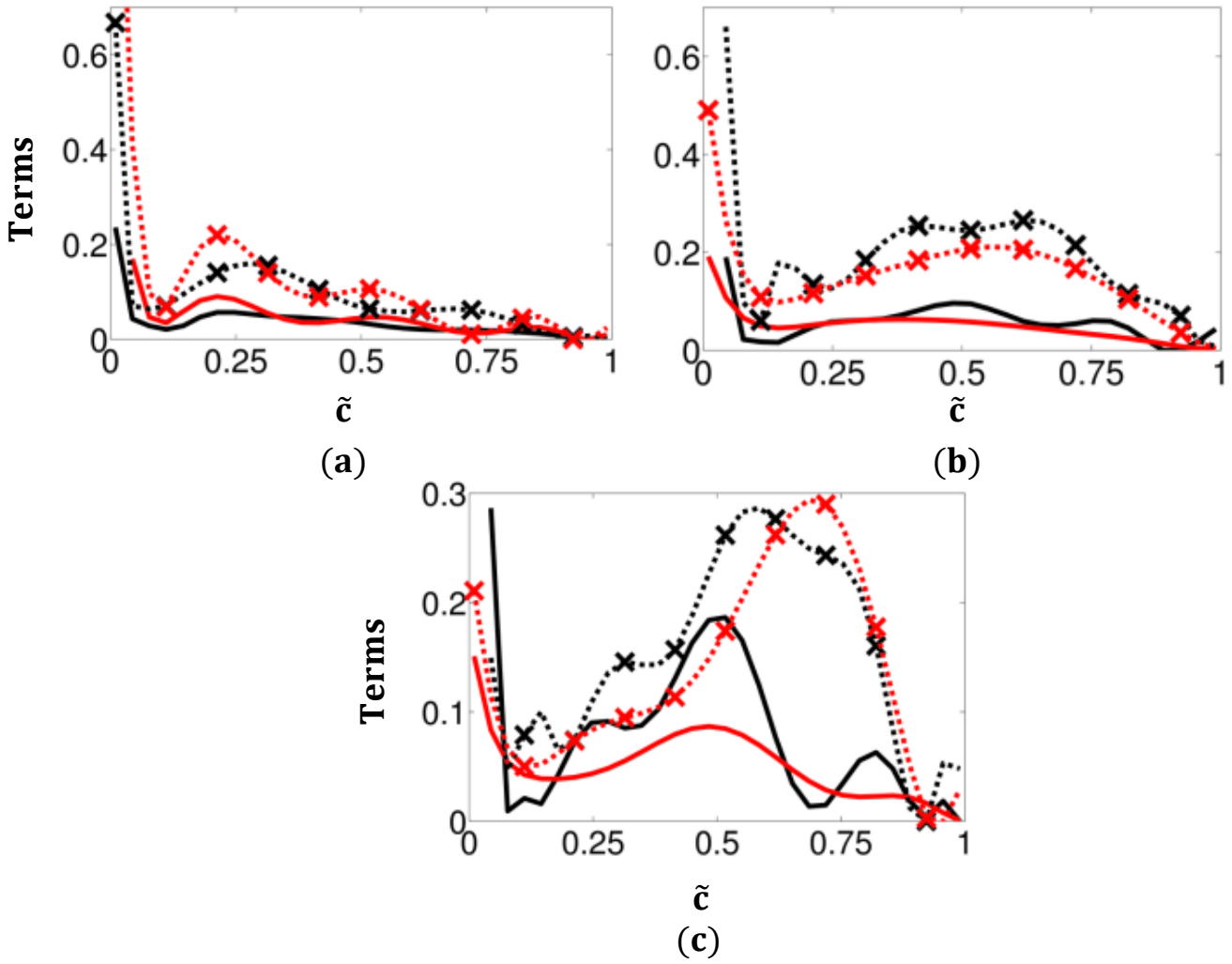

Fig. 6: Variation of $T_4 \times D_0/\rho_0 Y_{Fst}^2 S_{b(\phi_g=1)}^2$ [black] and the prediction of $\bar{\rho} C_{T_4} (\tilde{\epsilon}/\tilde{k}) \widetilde{\xi''^2}$ (for $C_{T_4} = 9.0$) [red] with $\tilde{c}$ for $a_d/\delta_{th} =$ (a) 0.06, (b) 0.08, (c) 0.10 and $\phi_d = 1.0$ (solid line), 1.7 (dashed line with crosses).

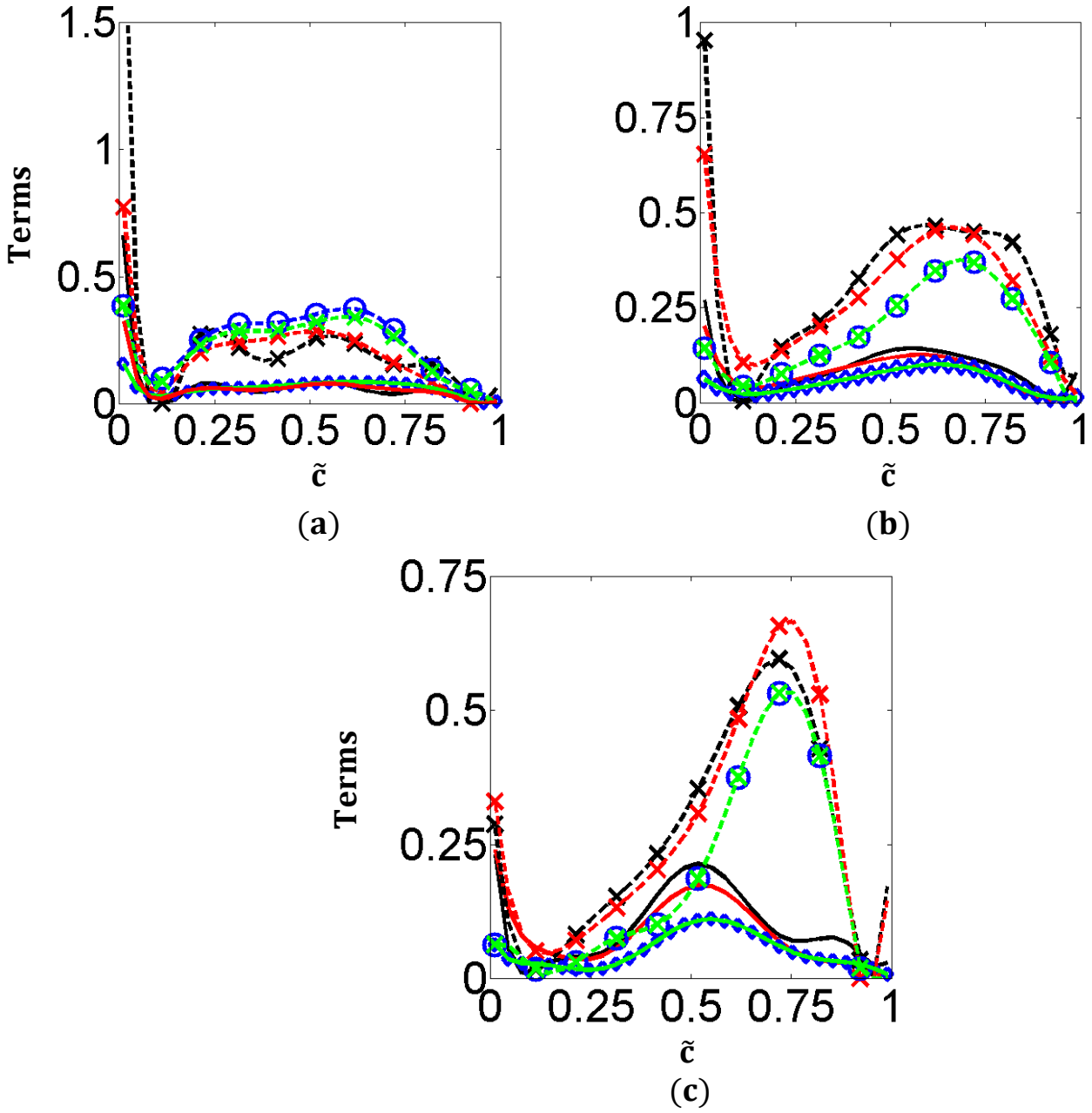

Fig. 7: Variation $\tilde{\epsilon}_Y \times D_0/Y_{Fst}^2 S_{b(\phi_g=1)}^2$ [black] and the predictions of SDY-LR, SDR-M1 and SDR-M2 [red, blue, green] with $\tilde{c}$ for $a_d/\delta_{th} =$ (a) 0.06, (b) 0.08, (c) 0.10 and $\phi_d = 1.0$ (solid line for DNS, SDY-LR and SDR-M2, and solid line with diamonds for SDR-M1), 1.7 (dashed line with crosses for DNS, SDY-LR and SDR-M2, and dashed line with circles for SDR-M1).